Drive Level Parameter Identification of an Induction Motor

Andreas Bünte Alex Hald Andreas Kirsch
University of Applied Sciences
Interaktion 1
33619 Bielefeld, Germany
Phone: +49 (521) 106-0
Email: andreas.buente@fh-bielefeld.de
URL: http://www.fh-bielefeld.de

Keywords

≪Induction motor≫, ≪Estimation technique≫, ≪System identification≫, ≪Magnetic saturation≫.

Abstract

A method to identify the electrical parameters of an inverter-fed induction motor is presented, which determines the saturation characteristic of the mutual inductance and the other parameters separately. Current displacement effects are taken into account. An advantage of this scheme is the insensitivity to voltage errors of the inverter. To achieve this, the identification of the constant parameters is based on the fact that the inverter primarily influences only the real part of the impedance. For the identification of the saturation characteristic, the impedance difference for 2 different but closely spaced frequencies is evaluated for different magnetic operating points.

Introduction

Models of the induction motor used for drive control include at least four parameters (stator resistance R_S, rotor resistance R_R, mutual inductance L_m and leakage inductances $L_{S\sigma} = L_{R\sigma}$) (cf. Fig 1 a)). The parameters R_S, R_R and $L_{R\sigma,S\sigma}$ are assumed to be constant and the number of pole pairs is assumed to be known. For the setting of the magnetic operating point, which is determined by the flux-forming component, the stator current or when the machine is used in a wide field weakening range, the saturation behavior of the mutual inductivity $L_m = f(i_\mu)$ should be known. The knowledge of the iron loss resistance R_{fe} is not necessary but can be useful if, for example, an optimum operating point has to be set in view of losses in the partial load range. Due to the importance for the control of induction motors, there are focused research activities to determine these parameters, e.g. [2], [9] and [13]. The various methods can be classified according to whether they determine the parameters during operation (online) or whether during the commissioning of the drive (offline).

Online methods have the advantage that they can track variable parameters, e.g. the temperature dependent resistances. However, the quality of the results depends on the operating points and the dynamics with which the drive system is operated. Offline methods can be differentiated according to the area of application, whereby the justifiable effort varies:

- *Manufacturer Level Identification:* The comparatively greatest effort can be made in the manufacturing plant of the motor or drive system. In particular, measuring devices are available for the electrical quantities, for speed and for torque. The motor can be stimulated and mechanically loaded as desired, but this requires time-consuming mechanical integration into the test rig. This identification can be performed by specialized personnel.
- *Drive Level Identification:* In the simplest case, parameter determination is carried out by the means of the drive system alone, i.e. stimulation, measurement and evaluation are carried out with

the inverter and the associated control. For safety reasons, a rotation of the shaft is not allowed. The need for specialized personnel is not desired.

This paper focuses on drive level offline methods. Manufacturer level measurements, especially no-load and short-circuit measurements are used to verify the measurement results [5]. At standstill, the motor is supplied with small stator voltage and requires only small amounts of electrical power and energy for stimulation. However, for the determination of the saturation characteristic of the main inductance, the stator current must be of the level of the rated current magnitude.

Models of the Induction Machine

If the iron losses (R_{fe}) are not taken into account, the equivalent circuit 1 a) shows the electrical parameters of the induction machine required for the control. The equivalent circuit has five components, but the corresponding admittance is given by the frequency response

$$\underline{Y}_2(\mathrm{j}\omega) = \frac{1 + \mathrm{j}\omega b_1}{a_0 + \mathrm{j}\omega a_1 + (\mathrm{j}\omega)^2 a_2} \tag{1}$$

and has only four coefficients b_1, a_0, a_1 and a_2, which depend on the electrical parameters. Therefore, an additional assumption regarding the leakage inductances may be made without loss of the generality. Three variants in particular are common here:

- $L_{S\sigma} = L_{R\sigma}$: The assumption of equal leakage inductances is mostly used.
- $L_{S\sigma} = 0$: This assumption leads to the so-called Γ-equivalent circuit, which is often used for stator flux-oriented control methods.
- $L_{R\sigma} = 0$: This assumption leads to the so-called inverse-Γ-equivalent circuit.

If the iron losses are taken into account, the equivalent circuit has three independent energy stores; a 3rd order system with the frequency response

$$\underline{Y}_3(\mathrm{j}\omega) = \frac{1 + \mathrm{j}\omega b_1 + (\mathrm{j}\omega)^2 b_2}{a_0 + \mathrm{j}\omega a_1 + (\mathrm{j}\omega)^2 a_2 + (\mathrm{j}\omega)^3 a_3} \tag{2}$$

is obtained. The number of parameters is now in equilibrium and an assumption about the distribution of leakage inductances is not mathematically exact but is often made as an approximation.

Fig. 1 b) and c) take into account the current displacement or deep bar effects [3], [8]. For better clarity,

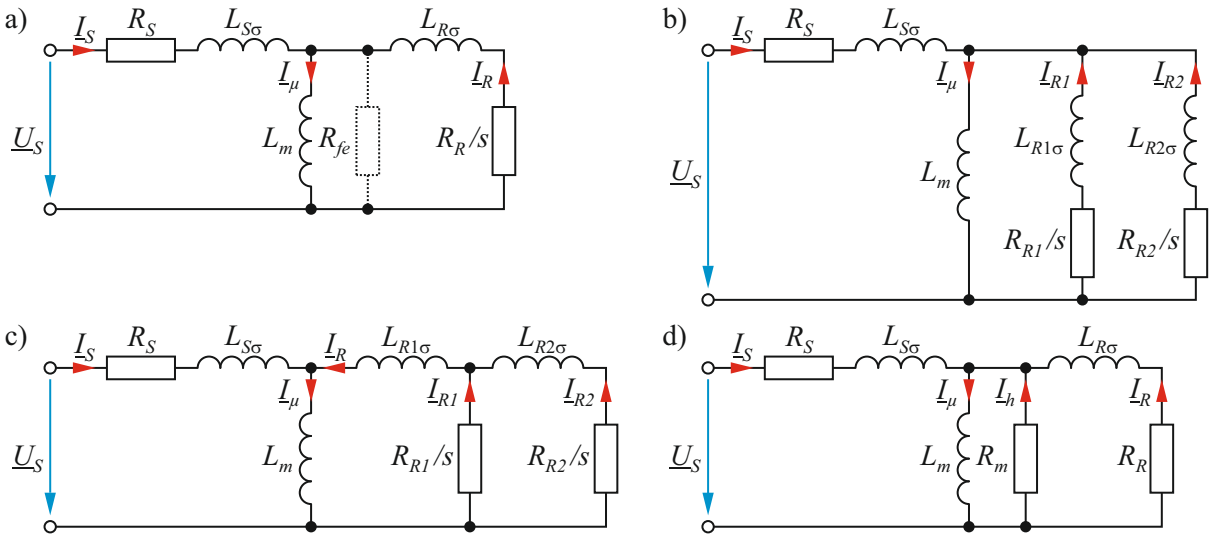

Fig. 1: Steady-state equivalent circuit of an induction motor a) with and without iron losses b) with current displacement, without iron losses, c) alternative form with current displacement, without iron losses, d) at standstill with one energized axis with combined iron losses and current displacement effects.

the same notation is used in both diagrams. With the exception of the stator resistance R_S, different parameters result for the different equivalent circuits. Both equivalent circuits can be described by the frequency response (2). The frequency response has six degrees of freedom while the equivalent circuits 1 b) and c) have seven. Analogous to the procedure for the inverse-Γ-equivalent circuit, the leakage inductance $L_{R1\sigma}$ in Fig. 1 d) can be assumed to be zero. As a consequence, R_{R1}/s is parallel to the mutual inductance L_m and, if the iron losses are also modeled, parallel to R_{fe}. By this, a separate determination of the iron losses and the current displacement effects is only possible if the slip s can be varied. If a rotation is not permitted, the slip is equal to 1 and corresponding resistances are combined ($R_m = R_{R1} \| R_{fe}$). The equivalent circuit Fig. 1 d) is obtained and since $R_{R1} \ll R_{fe}$ is valid the current displacement effects are dominant for R_m. With the exception of the Table II, space vector quantities in the amplitude invariant form are used in the following [7].

Since the motor must not produce any torque during identification, the rotor and stator flux vector must have the same direction. This behavior can be forced by energizing the motor only on a single axis. In the following the α-axis is regarded as the energized axis, $u_{S\beta} = 0$ and $i_{S\beta} = 0$ are valid. A standstill frequency response test (SSFR) is performed [6].

In this paper, the models Fig. 1 a) and d) are used. Therefore, the calculation of the electrical parameters from the frequency responses is given in Table I for both variants.

Table I: Calculation of the electrical parameters

Modell Fig. 1 a)	Modell Fig. 1 d)	
$R_S = a_0$	$R_S = a_0$	$L_{S\sigma} = \dfrac{a_3}{b_2}$
$R_R = \dfrac{a_1}{b_1} - a_0$	$R_h = \dfrac{a_2 b_2 - a_3 b_1}{b_2^2}$	$L_m = a_1 - \dfrac{a_3}{b_2}$
$L_m = \sqrt{\dfrac{(R_R b_1)(a_1 b_1 - a_2 - a_0 b_1^2)}{b_1}}$	$R_R = \dfrac{L_m^2 R_h}{(a_1 b_1 - a_2) R_h - L_m^2}$	$L_{R\sigma} = \dfrac{b_2 L_m R_h^2}{(a_1 b_1 - a_2) R_h - L_m^2}$
$L_{R,S\sigma} = R_R b_1 - L_m$		

According to [2], the single-axis supply differs from the operation with rotating fields with respect to the magnetization behavior. With rotating fields in the steady state (e. g. no-load test), the length of the space vector $|i_\mu|$ and also the flux $|\psi_m| = |L_m(i_m u) \cdot i_m|$ is constant. With sinusoidal currents in the single-axis test, the entire saturation characteristic is run through. Depending on the measuring method, a conversion of the saturation characteristics is therefore necessary.

Experimental setup

The rated data of the induction motor used are listed in Table II. To simplify the measurements and ensure a good accuracy, the machine was fed with an extra-low voltage inverter. This inverter is equipped with Vishay SIR622DP MosFETs, which are driven by Diodes Incorporated DGD0504FN-7 gate drivers. The electronics were supplied directly from a stabilized voltage source with $U_{dc} = 70$ V. The switching frequency is $f_S = 10$ kHz. LEM HO10-P/SP33 were used for the current measurement.

Since the machine was only stimulated with low frequencies or only with small amplitudes, the electronics do not reach their control limits despite the low dc link voltage. For this reason, the measurement methods described in this paper can be transferred to systems with mains voltage.

Measurement of the Constant Parameters

In [2], to determine the parameters of the model Fig. 1 a) without R_{fe}, the frequency response is measured by cross-correlation with sinusoidal currents and a single axis test. This method is suitable for the drive level.

Table II: Name plate data of motor

Parameter	Symbol	Value
Manufacturer	WEG Group	
Type	12463324	
Rated frequency	f_N	50 Hz
Rated power	P_N	3.0 kW
Rated voltage	U_N	400 V
Rated current	I_N	5.9 A
Rated speed	n_N	2880 min^{-1}
Rated power factor	λ_N	0.86

Table III: Electrical parameter of motor,

Mod. Fig. 1 a)			Mod. Fig. 1 d)	
Par.	Lock. Rot. No-Load	SSFR	Par.	SSFR
R_S	2.52 Ω	2.91 Ω	R_S	2.90 Ω
R_R	1.65 Ω	1.29 Ω	R_m	2.53 Ω
L_m	272 mH	47.37 mH	R_R	1.21 Ω
$L_{R,S\sigma}$	8.83 mH	13.42 mH	L_m	43.63 mH
R_{fe}	1570 Ω	–	$L_{S\sigma}$	20.65 mH
			$L_{R\sigma}$	10.97 mH

The voltage source inverter has some parasitic effects, that causes differences $\Delta u_S = u_S - u_S^*$ between reference and actual voltage. The voltage change is especially large when current zero crossings occur. To avoid this, a DC component is superimposed on the current, e. g. $i_{S\alpha} = \bar{i} + \hat{i}\sin\omega t = I_N/\sqrt{2} + \frac{\sqrt{2}}{10} I_N \sin\omega t$.

The remaining voltage error influences the parameter identification if voltage detection is not used. One error is caused by the switching lag times which are necessary to avoid short-circuits at the inverter. This results in a difference between the reference duty cycle and the real duty cycle dependent on the tum-on-delay, the turn-off-delay and the signs of the phase currents. This error depends on the phase currents and the junction temperature. The same is true for the forward losses of the IGBTs and diodes of the inverter. If the temperature dependence is neglected, the voltage error uniquely depends on the current and corresponding describing function $\Delta U_S(\text{j}\omega)/I_S(\text{j}\omega)$ is real, as shown in [2]. Furthermore, if the current amplitude and offset is constant for different frequencies, the real part of the corresponding describing function is real and constant. By this, the inverter error voltage affects the stator resistance and the determination of $L_{S\sigma}$ and R_R are not influenced by the inverter. The determination of the saturation characteristic is not possible with constant current amplitude and offset and is done in a second step.

The proposed measurement was reproduced for a motor according to Table II. The frequencies were varied in the range 0.1 Hz $\leq f \leq$ 1000 Hz. The measurement was performed on the heated motor. Then the measurement data were approximated by the 2nd order model (Eq. (1)) and the 3rd order model (Eq. (2)). Fig. 2 shows the results and Table III the parameters of the motor according to Table I. The following effects can be observed:

- Since the conductance were approximated, and its magnitudes become small for high frequencies, the model uncertainties have an effect mainly at high frequencies.
- The inverter has a significant influence on the stator resistance.
- Higher frequencies yield to model uncertainties, which can be reduced with the 3rd order model. This model does not completely eliminate the model uncertainties; deviations can be observed from about 100 Hz. For an improvement, further increasing the order is possible. Retiere [10] proposes the use of a noninteger order model.
- The calculated mutual inductances differ strongly from the no-load test and are unreliable. The deviations can be explained: With regard to the magnetic behavior, the excitation selected for this measurement leads to the passage of minor loops. Their slopes differ significantly from those of the major loops determined in the no-load test [1].
- The rotor resistance obtained with the locked-rotor test is 21.8 % higher than the value obtained with the SSFR test. The short circuit test was performed at 50 Hz. In the SSFR measurement, smaller frequencies are weighted more heavily, at which the current displacement effects are smaller. The plausibility could be shown with a locked-rotor test with a smaller feed frequency. With the 3rd model, R_R is further decreased.
- The value for R_m obtained with the 3rd order model is in the order of magnitude of the stator resistance. Obviously, it models not only the iron losses but primarily current displacement effects.
- The estimated values of the leakage inductances are significantly larger with the SSFR test than

the value of the locked-rotor test. The data of the locked-rotor test were determined with rated current. A comparative measurement with the mean value of the SSFR test resulted in a higher value, i.e. the leakage inductance for the motor under test shows significant saturation influences, which makes the comparability of the data difficult.

The frequency response measurement was performed in a range of 0.1 Hz $\leq f \leq$ 1000 Hz with the aim to show the model inaccuracies. These high frequencies are not necessary for parameter identification. Estimation with the 3rd model provides stable values when measured up to about 200 Hz, and for the 2nd model measurements up to about 80 Hz are sufficient. Furthermore, the number of measurements can be limited to approximately $n_f = 10$.

For the field-oriented control of the induction motor, the 2nd order model is usually used, since the iron losses do not significantly affect the dynamics and the current displacement effects are not important due to the small slip frequencies. However, by comparing the values of both models, conclusions can be drawn as to how pronounced the current displacement effects are. Further optimization of the drive control may be possible as a result [11], [12]. The iron losses and the current displacement effects cannot be separated at standstill. If the exact knowledge of the iron losses and the current displacement effects becomes necessary, the identification should be made on manufacturer level or with suitable online procedures.

Measurement of the Mutual Inductance

Zero torque during the measurement can be met with the single-axis test. For the determination of the main inductance, two difficulties are associated with the single-axis test:

- At standstill, the determination of the saturation characteristic is difficult. Since $s = 1$ applies, the frequency must not be too high, otherwise the small rotor impedance will short-circuit the comparatively high-impedance mutual inductance. Due to this, the motor is fed only with small voltage. If the excitation is done with the inverter and a voltage measurement is not available the

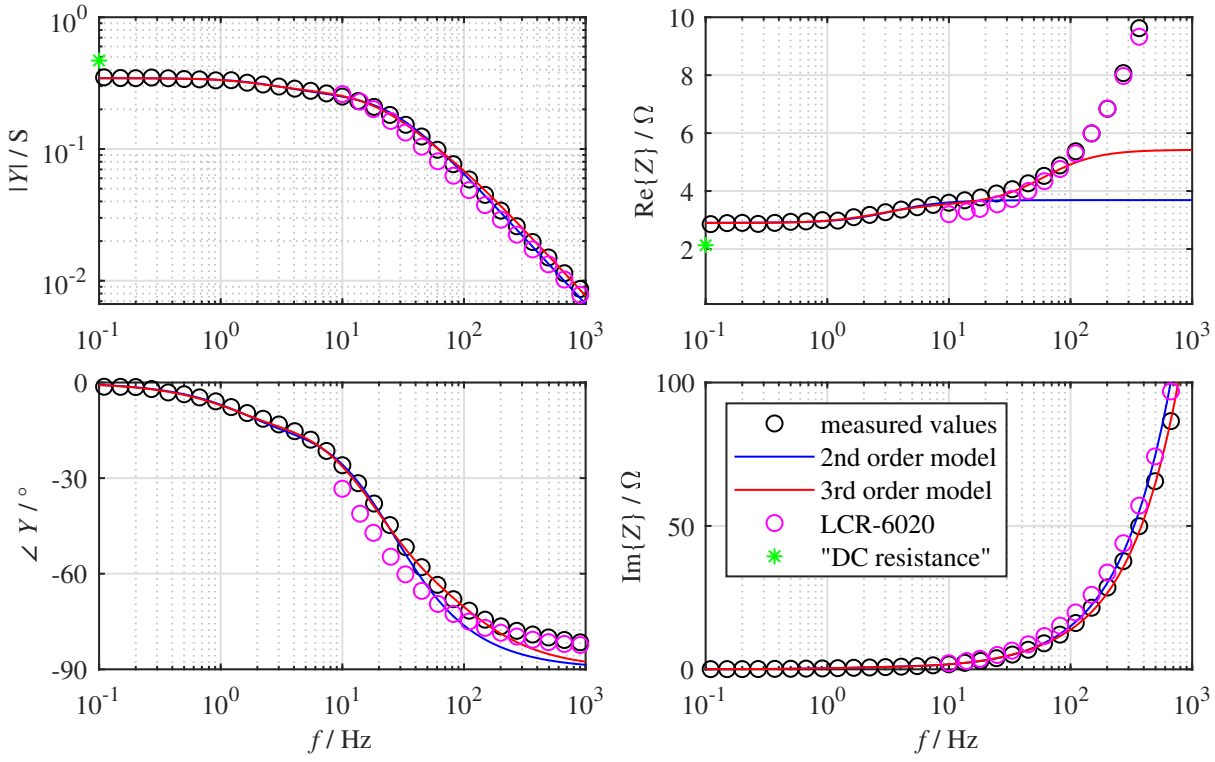

Fig. 2: Measured conductance and impedance (hot induction motor) and fitted models. Verification (DC and $f \geq 10$ Hz) is done with an LCR meter (GW Instek) and a cold induction motor. For the sake of visualization, the DC value is shown at 0.1 Hz.

results are seriously distorted by the fault voltage caused by the inverter.
- The magnetic use of the motor in single-axis operation differs from the use in rotating field operation. A conversion of the respective characteristic curves becomes necessary.
- An evaluation of the real part alone is not useful, because the stator resistance must be known exactly (cf. (7)), which is not possible in view of the converter effects.

Comparison of Magnetizing Curves

For the operating point adjustment of the asynchronous motor, the saturation characteristic determined with the no-load test is used. In the no-load test, the magnetizing current can be set with variable stator voltage and thus a characteristic curve $L_m(i_\mu)$ can be determined. During a no-load measurement, the motor operates with a rotating flux whose amplitude is constant. The same applies to the magnetizing current $|i_\mu| = \sqrt{(i_{S\alpha} + i_{R\alpha})^2 + (i_{S\beta} + i_{R\beta})^2}$, which depends on the stator and rotor currents. This magnetizing current determines the instantaneous magnetic operating point.

In the case of single-axis supply, the magnitude of the magnetizing current is not constant and depends on the test signal. In the following, sinusoidal test signals without offset are considered. When an offset is used, from a magnetic point of view a minor-loop is passed through. The properties of this minor-loop do not allow a simple conclusion to be made about the main loop. If only the fundamental component is evaluated during the single-axis test, a fundamental inductance $L_{fm}(\widehat{I_\mu})$ is determined. For this inductance, the entire covered range of the magnetization characteristic is relevant. An approximate conversion of the saturation characteristic is introduced in [2] and used in the following.

It could be assumed that the function $L_m(i_\mu)$ is even. If the saturation curves could be fitted by the polynomials

$$L_m(i_\mu) = \sum_{n=0}^{N} a_n {i_\mu}^n \tag{3}$$

$$L_{fm}\left(\widehat{I_\mu}\right) = \sum_{n=0}^{N} a_{fn} {\widehat{I_\mu}}^n, \tag{4}$$

the coefficients satisfy the equation

$$a_{fn} = k_n \cdot a_n \tag{5}$$

with

$$k_n = \begin{cases} 2 \prod_{l=0}^{n/2} \frac{2l+1}{2l+2} & \text{if } n \text{ even} \\ \frac{4}{\pi} \prod_{l=1}^{(n+1)/2} \frac{2l}{2l+1} & \text{else} \end{cases} \tag{6}$$

Identification of the inductance with the imaginary part

In [2] the authors suggested to evaluate only the imaginary parts of the impedance (Fig. 1 a) with $L_{S\sigma} = L_{R\sigma} = L_\sigma$ and $L_m = f(\widehat{i_\mu})$)

$$\underline{Z}_2(L_m, \omega) = \frac{1}{\underline{Y}_2(\omega)} = R_S + \frac{R_R (\omega L_m)^2}{R_R^2 + \omega^2 (L_m + L_\sigma)^2} + \mathrm{j} \left(\omega (L_m + L_\sigma) - \frac{\omega^3 L_m^2 (L_m + L_\sigma)}{R_R^2 + \omega^2 (L_m + L_\sigma)^2} \right) \tag{7}$$

measured at different current levels for the determination of the saturation characteristic, since the imaginary parts are largely not influenced by the inverter. The measurements were performed at low frequencies, ensuring good sensitivity of the imaginary parts from the main inductance. For these frequencies,

the 2nd order model is sufficiently accurate. For one current level the mutual inductance is given with:

$$L_m\left(\widehat{I}_\mu\right) = \frac{R_R^2 - \omega^2 L_\sigma^2 - \sqrt{\left(R_R^2 - \omega^2 L_\sigma^2\right)^2 + 4R_R^2 \mathrm{Im}\left\{\underline{Z}_2\right\}\left(2\omega L_\sigma - \mathrm{Im}\left\{\underline{Z}_2\right\}\right)}}{2\omega \mathrm{Im}\left\{\underline{Z}_2\right\} - 4\omega^2 L_\sigma} - L_\sigma \tag{8}$$

Here the magnetizing current depends on the stator current and the frequency.

$$\widehat{I}_\mu = \widehat{I}_{Sd}\sqrt{\frac{R_R^2 + \omega^2 L_\sigma^2}{R_R^2 + \omega^2\left(L_m + L_\sigma\right)^2}} \tag{9}$$

According to [2], a suitable measurement frequency can be determined with the relative sensitivities

$$E_x(\omega) = \frac{\partial \mathrm{Im}\left\{\underline{Z}_2\right\}}{\partial x} \cdot \frac{x}{\mathrm{Im}\left\{\underline{Z}_2\right\}} \tag{10}$$

of the evaluated imaginary part. The imaginary part should depend as much as possible on the inductance and as little as possible on the remaining parameters. The results are shown in Fig. 3. The measurement frequency should be to the left of the intersection of the sensitivities E_{Lm} and E_{RR}. Measurement errors in leakage inductance only have an effect at significantly higher frequencies and are less critical. For the following investigations $f = 0.2$ Hz was used.

Very good results were obtained for various motors using this method. However, for motors with larger power ratings, two problems can be observed:

- Due to the large rotor time constants and the associated small measurement frequencies, the total measurement time becomes very large.
- Residual errors of the inverter also affect the imaginary part of the measured impedance. Due to the small impedances of high motor powers, the inductances are therefore estimated too small.

Very good results were obtained for various motors using this method.

Identification of the inductance with double frequency measurement

In this paper, a new approach to determine the main inductance by the difference $\Delta\underline{Z}(L_m) = \underline{Z}(L_m, \omega_2) - \underline{Z}(L_m, \omega_1)$ is presented. This double frequency measurement results in interesting features:

- The result is independent of R_S. Measurement errors in this quantity have no effect.
- If the stator current amplitude $\widehat{i}_S$ is the same for both frequencies and the inverter errors are only weakly frequency-dependent, the inverter errors are also suppressed. This applies to both the real and imaginary parts.
- Two measurements are required for one point of the saturation curve. The total measurement time becomes longer.
- If the stator current amplitude $\widehat{i}_S$ is the same for both frequencies, the magnetizing current will be different for the two frequencies.
- The choice of frequencies $\omega_{1,2}$ represent degrees of freedom.

The determination of the frequencies is critical. Therefore, this selection is considered below. When choosing the frequencies, the following must be taken into account:

- The frequencies should not differ too much, otherwise the magnetizing currents will differ significantly and thus different operating points of the characteristic curve will be measured for both frequencies.
- The frequency difference should not be too small, otherwise $\Delta\underline{Z}_{meas}$ cannot be measured robustly.
- The frequencies must not be too high, otherwise the rotor circuit becomes dominant.
- The frequencies should not be too small, otherwise the total measurement time becomes unattractively large.

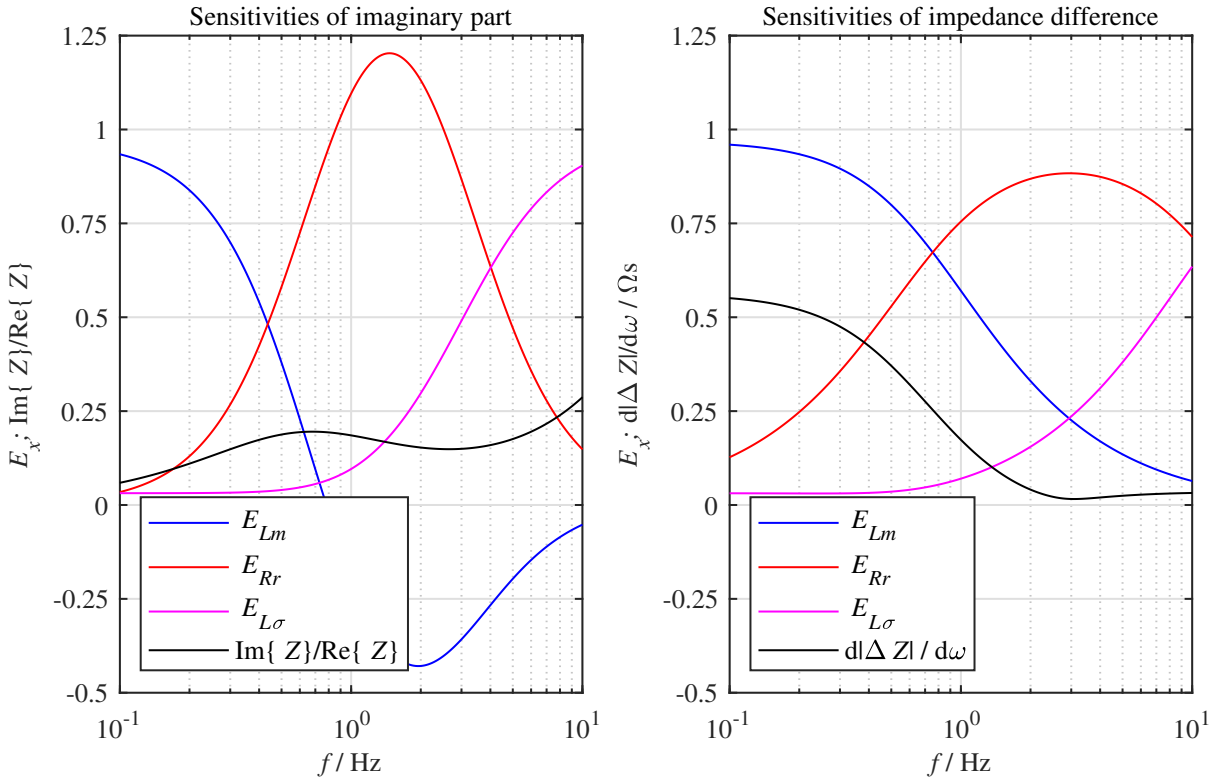

Fig. 3: Relative sensitivities of $\mathrm{Im}\{\underline{Z}_2\}$ (left) and of $|\underline{Z}_2(\omega_2) - \underline{Z}_2(\omega_1)|$ (right). For further consideration of the obtainable accuracies, the ratio of the imaginary and real parts as well as the derivation according to the frequency are additionally shown.

Also for this measurement the absolute frequencies can be determined by means of the relative sensitivities. These are determined with the equation

$$E_x(\omega) = \frac{\partial|\Delta\underline{Z}(L_m)|}{\partial x} \cdot \frac{x}{|\Delta\underline{Z}(L_m)|} \tag{11}$$

and shown in Fig. 3 (right). In this case, measurement errors in leakage inductance only have an effect at significantly higher frequencies and are less critical. The measurement frequencies should be to the left of the intersection of the sensitivities E_{Lm} and E_{RR}. For this method, the intersection point is at higher frequencies than for the determination via the imaginary part. By this, the disadvantage of a double measurement can be compensated by the choice of a higher frequency. Proven choice in simulations with different motors is:

$$\omega_1 = (0.2 \ldots 0.4) \cdot \frac{R_R}{L_m} \tag{12}$$

For a comparability of the results $\omega_1 = 2\pi \cdot 0.2\ \mathrm{s}^{-1}$ is chosen also here. The remaining degree of freedom is the frequency difference $\Delta\omega = \omega_2 - \omega_1$. Measurements on the test rig show that the quality of the results depends strongly on this difference frequency. The practical results in this paper are obtained for $\omega_2 = 1.1 \cdot \omega_1$.

With the measured difference $\Delta\underline{Z}_{meas}$, the inductance L_m can be determined by solving the equation $0 = \underline{Z}_2(L_m, \omega_2) - \underline{Z}_2(L_m, \omega_1) - \Delta\underline{Z}_{meas}$. However, due to measurement errors and differences in magnetizing current, this equation is not expected to be simultaneously satisfiable for the real and imaginary parts at the same time. Instead, the cost functional

$$J(L_m) = |\underline{Z}_2(L_m, \omega_2) - \underline{Z}_2(L_m, \omega_1) - \Delta\underline{Z}_{meas}|^2 \tag{13}$$

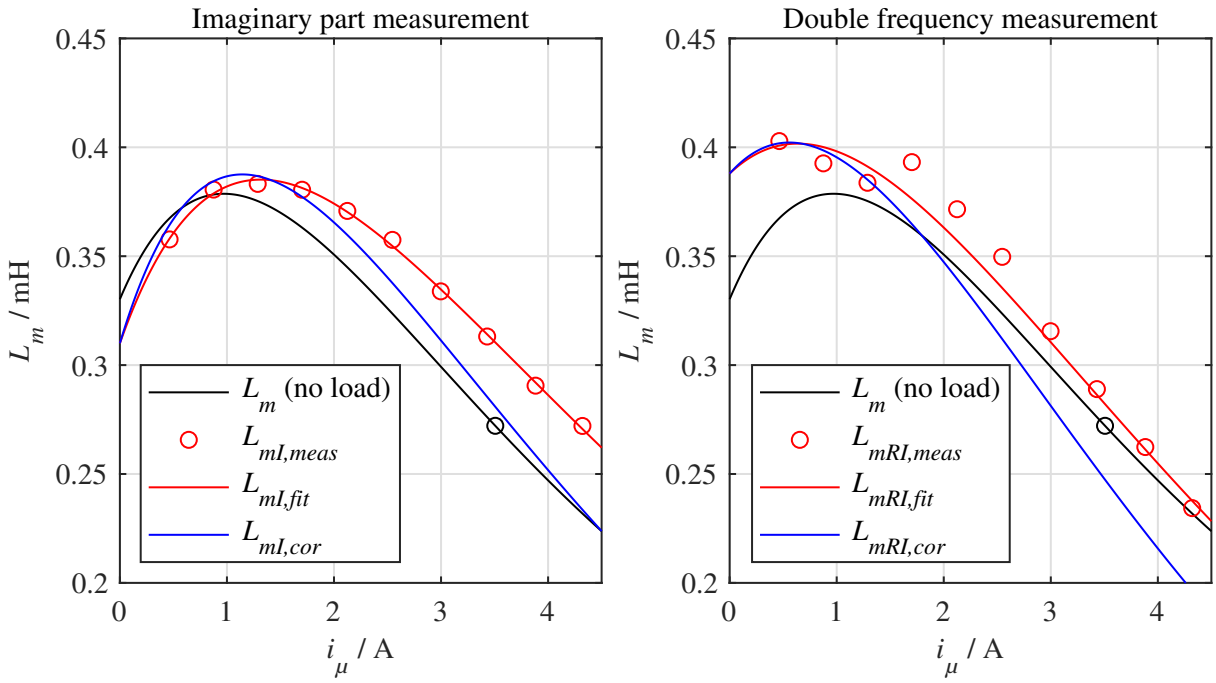

Fig. 4: Magnetizing curves of the one-frequency test (left) and the double frequencies test (right). L_m is the result of the no-load test, $L_{mI,mRI}$ are the results of the different tests and $L_{m,cor}$ are the results of the transformation according to (3)–(6). The rated magnetizing point is marked.

is minimized using numerical optimization. This cost functional describes the distance between the measured difference and the calculated difference in the complex plane and the minimum provides an estimation for L_m.

With regard to the suppression of the influence of the voltage errors of the inverter, the stator current amplitude should be kept constant. Then, the magnetizing currents differ depending on the two measuring frequencies (cf. (9)). With the choice $\omega_1 = 2\pi \cdot 0.2\,\mathrm{s}^{-1}$; $\omega_2 = 1.1 \cdot \omega_1$, the difference for the magnetizing current for the motor under test is less than 1.5 % and negligible. In the following, the average value of the magnetizing currents at both frequencies is assigned to the calculated inductance.

Practical results of mutual inductance identification

Fig. 4 shows the measurement results for the motor according to Table II. The no-load characteristic curve describes the instantaneous values and can be considered as the reference. For both methods, the fundamental inductance was measured for 10 different stator current amplitudes and the measuring points were fitted with a polynomial. Since the characteristics of the fundamental inductance correspond to the single-axis supply, they must be converted to the no-load characteristic using equations (3)–(6). $L_{mX,cor}$ are the final results.

The following can be noted:

- In view of a drive level identification a measurement of the saturation characteristic is possible with both methods.
- For this setup, the results are better with the evaluation of the imaginary part alone. For the rated magnetizing current, there is a deviation of 3.3 % for the mutual inductance in this case and a deviation of -9.1 % for the double-frequency measurement.
- The measurement via the imaginary part for small currents seems to be more robust than the differential evaluation. This behavior could not be improved by increasing the frequency spacing $\Delta\omega$.
- The measurement at one frequency takes about 10 s. With large stator currents, the winding temperature can increase noticeably and influence the resistance. Thus, the sequence of measurements has an influence on the results.

Conclusion

An identification scheme was presented that allows parameter identification of an induction motor at standstill. In a first step the values of the resistances and the leakage inductances are determined by a frequency response test for both, a 2nd order and 3rd order model. The 3rd order model considers current displacement effects. These effects can be modeled with a combined resistor R_m which includes also iron losses. The 3rd model can be used to represent the system behavior up to much higher frequencies. Whether this is useful depends on the control method used.

In a second step, the saturation-dependent main inductance was determined. For this purpose, a new method was presented in which the differential impedance of two frequencies is evaluated. Inverter influences can thus be partially suppressed. The principle function of the presented method could be confirmed with measurements. In comparison with a known method, in which only the imaginary part of the impedance is evaluated, the robustness does not yet seem to be optimal. Further research is needed to improve this behavior.

References

[1] Bünte, A. and Grotstollen, H.: Parameter Identification of an Inverter–Fed Induction Motor at Standstill with a Correlation Method, 5. Eur. Conf. on Power Electronics and Applications (EPE), vol. 5, Brighton: 1993, pp. 97–102.

[2] Bünte, A. and Grotstollen, H.: Offline Parameter Identification of an Inverter–Fed Induction Motor at Standstill, 6. Eur. Conf. on Power Electronics and Applications (EPE), vol. 3, Sevilla: 1995, pp. 492–496.

[3] Corcoles, F.; Pedra, J.; Salichs, M. and Sainz, L.: Analysis of the induction machine parameter identification, IEEE Transactions on Energy Conversion, vol. 17, no. 2, 2002, pp. 183–190.

[4] Grotstollen, H. and Wiesing, J.: Torque capability and control of a saturated induction motor over a wide range of flux weakening, IEEE Transactions on Industrial Electronics, vol. 42, no. 4, 1995, pp. 374–381.

[5] IEEE: IEEE Standard Test Procedure for Polyphase Induction Motors and Generators, IEEE Std 112, 2017.

[6] IEEE: IEEE Guide for Test Procedures for Synchronous Machines, IEEE Std 115, 2009.

[7] Leonhard, W.: 30 Years Space Vectors, 20 Years Field Orientation, 10 Years Digital Signal Processing with Controlled AC-Drives, a Review, EPE Journal, vol. 1, 1991, pp. 13…20, 89…102.

[8] Monjo, L.; Kojooyan-Jafari, H.; Corcoles, F. and Pedra, J.: Squirrel-Cage Induction Motor Parameter Estimation Using a Variable Frequency Test, IEEE Transactions on Energy Conversion, vol. 30, no. 2, 2015, pp. 550–557.

[9] Odhano, S. A.: Self-Commissioning of AC Motor Drives, PhD thesis, Politecnico di Torino, Turin, 2014.

[10] Retiere, N. M., Ivanes, M. S.: An Introduction to Electric Machine Modeling by Systems of Noninteger order. Application to double-cage induction machine, IEEE Transactions on Energy Conversion, vol. 14, no. 4, 1999, pp. 1026–1032.

[11] Seok, J. K., Sul, S. K.: Pseudorotor-Flux-Oriented Control of an Induction Machine for Deep-Bar-Effect Compensation, IEEE Transactions on Industry Applications, vol. 34, no. 3, 1998, pp. 429–434.

[12] Schubert, M.; Koschik, S.; De Doncker, R. W.: Fast Optimal Efficiency Flux Control for Induction Motor Drives in Electric Vehicles Considering Core Losses, Main Flux Saturation and Rotor Deep Bar Effect. Application to double-cage induction machine, Annual IEEE Applied Power Electronics Conference and Exposition (APEC), 2013, pp. 811–816.

[13] Toliyat, H. A.; Levi, E. and Raina, M.: A review of RFO induction motor parameter estimation techniques, IEEE Transactions on Energy Conversion, vol. 18, no. 2, 2003, pp. 271–283.